RSC Applied Polymers

ROYAL SOCIETY OF CHEMISTRY

PAPER

View Article Online
View Journal | View Issue

Cite this: *RSC Appl. Polym.*, 2025, **3**, 1183

Reversible B–O bond-based epoxy vitrimers with high thermomechanical and dynamic properties enhanced by intermolecular B–N coordination

Qi Li, *†[a] Dong Wang,†[a] Tianjiao Wang,[a] Yang Zhang,[a] Shiyang Liu,[b] Shiwei Zhang,[a] Zhufeng Hu,[a] Liying Li,[a] Guoyong Wang[a] and Yingmin Zhao[a]

Received 17th May 2025,
Accepted 6th August 2025

DOI: 10.1039/d5lp00144g

rsc.li/rscapplpolym

The development of recyclable and self-repairable vitrimer materials featuring reversible B–O bonds has garnered increasing attention. However, their stability and thermomechanical properties remain insufficient for engineering applications in reusable carbon fiber-reinforced composites (CFRCs). Herein, we report a high-performance epoxy vitrimer containing boronic ester bond-based dynamic exchange networks, to which a small amount of N-donating imidazole has been added for introducing intermolecular N–B coordination interactions. The obtained vitrimer (**E51-NBO-IMZ**) possessed a high glass transition temperature (T_g) of 198 °C and tensile modulus of 3.71 GPa. Compared to the system without imidazole, it exhibited significantly improved solvent resistance due to the stabilization effect of N–B coordination on the B-center atoms. Moreover, stress relaxation tests also indicated a lower activation energy (E_a = 151.31 kJ mol^{-1}) of the **E51-NBO-IMZ** vitrimer, suggesting better dynamic exchange activity. Despite the high stability and improved thermomechanical properties, the self-repairing, recycling and degradation of the vitrimer and its CFRCs were successfully achieved under heating, stress or chemical environmental conditions, showing outstanding potential for practical applications.

1. Introduction

Thermosetting polymer materials and their composites, characterized by low density, superior mechanical properties and exceptional environmental stability, have found extensive applications in the automotive, wind power and aerospace industries.[1–4] Nevertheless, the rapid increase in the usage of thermosetting polymers has engendered significant resource cost pressure and environmental contamination, which is primarily attributable to their inherent non-degradability and non-processability of covalent cross-linked networks.[5–7] To address the above challenges, novel materials featuring covalent adaptable networks (CANs), named vitrimers, have been developed to construct sustainable polymeric materials and composites with recyclable, processable and repairable properties.[8–13] Hence, vitrimers have been considered as the third category of polymeric materials alongside traditional thermoplastics and thermosets.[14,15] Among them, epoxy vitrimers have garnered the most research attention due to their rich designability, superior mechanical performance and application potential.[16–19]

In recent years, a diverse range of dynamic covalent reactions has been successfully applied in the design and fabrication of CAN-based epoxy vitrimers, such as transesterification,[20–22] disulfide exchange,[23,24] imine exchange,[25–27] siloxane exchange,[28–30] Diels–Alder reaction,[31–33] *etc.* Such dynamic chemical bonds can undergo reversible dissociation and reformation under external stimuli (*e.g.* high temperature, UV radiation, pressure, pH, and catalytic agents), thereby enabling self-healing and rearrangement of polymeric networks. However, the majority of epoxy vitrimers exhibit certain limitations: first, the initiation of some vitrimers requires the incorporation of large amounts of catalyst or use of very high temperature and pressure.[34,35] Besides, the introduction of vulnerable dynamic structures usually leads to the weakening of thermal oxygen and chemical stability, as well as mechanical properties.[36,37] These drawbacks have strongly affected the advancement and practical application of epoxy vitrimers. Consequently, it remains challenging to develop high performance epoxy vitrimers with enhanced mechanical properties, high stability and adequate dynamic capability.

Reversible B–O bonds, mainly synthesized through the dehydration condensation reaction between boronic acids and diols or the trimerization of boronic acids, are an emerging

[a]*Aerospace Institute of Advanced Materials & Processing Technology, Beijing, 100074, China. E-mail: liqi032377@163.com*
[b]*China International Engineering Consulting Corporation, Beijing, 100089, China*
† These authors contributed equally to this work.

kind of dynamic bond in the construction of vitrimers.[38–43] On account of the sensitive sp^2 hybridized electron-deficient boron atoms, these bonds easily undergo reversible dissociation–association reactions without catalysts upon changing the chemical environment and temperature. To date, numerous efforts have been devoted to fabricate B–O bond-based vitrimers, yet most reported systems have been elastomers or low-modulus polymers for the consideration of fast exchange reactions.[44–46] Recently, the use of boronic ester bonds to modify epoxy resins for the construction of high performance vitrimers has been a new research hot-spot. For instance, Zhang *et al.*[47] reported an epoxy vitrimer based on a phenyl boric acid curing agent for green degradation, closed-loop recycling, and ready reprocessing, which exhibited good thermal and mechanical properties. Zeng *et al.*[48] reported epoxy networks that were fabricated through the reaction between a thiol curing agent containing borate esters and a rosin-derivate containing an epoxide group. The epoxy networks displayed effective reprocessing properties with a high degree of recovering mechanical properties. Despite the significant progress in the preparation and dynamic exchange performance of epoxy vitrimers based on B–O bonds, their environmental degradation resistance, thermal resistance, and mechanical properties required further improvement. Moreover, their application in reusable CFRCs needed further verification.

Notably, a series of research studies have proved that the intra/intermolecular dative N–B interactions gave rise to a structural transformation of boron heterocycles from trigonal planar to tetrahedral, which enhanced the hydrolytic stability of the central boron atom.[49–51] Thus, the formation of N–B coordination can be utilized to promote the stability of boronic ester linkages and confer improved mechanical properties of vitrimers. Li *et al.*[52] reported the study of an epoxy resin reacting with a trifunctional amine containing an N–B coordinated boronic ester. Owing to the N–B coordinated structure, the dynamically cross-linked epoxy resin possessed good water and humidity resistance. Furthermore, the N–B coordination interaction was reported to be effective for accelerating the dynamics of the transesterification of boronic esters and beneficial for the self-healing performance.[53,54] Song *et al.*[55] reported the synergy between the boronic ester and N–B coordination to improve the mechanical properties and the self-healing efficiency in polyurethane vitrimers. In this work, the N–B coordination not only accelerated the reshuffling of the boronic ester at room temperature, but also dramatically enhanced the mechanical properties.

Herein, we represent an effective strategy for constructing high performance epoxy vitrimers by introducing borate ester-based cross-linking groups and intermolecular N–B coordination (Fig. 1). To achieve the fabrication of high-performance epoxy vitrimers, a diamine curing agent containing a pair of borate ester bonds (**NBO**) was designed and synthesized, and used for the cross-linking of a typical bisphenol A epoxy monomer (**E51**). In order to introduce the N–B coordination and stabilize the B–O dynamic covalent bonds, a minimal quantity of imidazole (**IMZ**) was added, which concurrently functioned as an N donor and cross-linking reaction accelerator. For comparative analysis, an epoxy vitrimer without imidazole (**E51-NBO**) was also prepared. Characterization results showed that the incorporation of imidazole not only promoted the cross-linking reaction and increased the glass transition

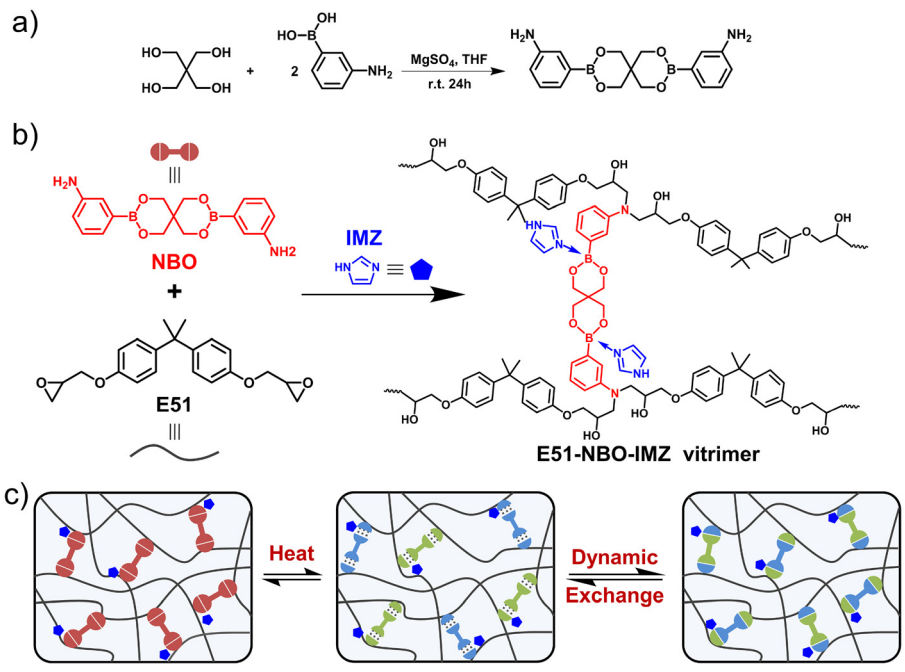

Fig. 1 Design concept: (a) synthetic route of the B–O bond-containing diamine curing agent **NBO**; (b) chemical structure of the **E51-NBO-IMZ** vitrimer; and (c) schematic illustration of the dynamic exchange process of the **E51-NBO-IMZ** vitrimer.

temperature (T_g), but also significantly improved the solvent resistance. Surprisingly, despite the vitrimer with imidazole (**E51-NBO-IMZ**) exhibiting superior thermomechanical properties, the stress relaxation test indicated that its activation energy (E_a) was also lower, suggesting a better dynamic exchange activity at elevated temperatures. Taking advantage of the effective B–O bond-based cross-linking networks, we successfully prepared a high performance epoxy vitrimer and its carbon fiber-reinforced composites with excellent recyclability, degradability and self-repairing properties.

2. Experimental

2.1 Materials

3-Aminophenylboronic acid, pentaerythritol and magnesium sulfate were purchased from Innochem. Analytically pure tetrahydrofuran, dichloromethane, petroleum ether, acetone, ethanol, deionized water, *N*,*N*-dimethylformamide and other solvents were commercially available and used as supplied without further purification. The **E51** epoxy resin was purchased from Sinopec.

2.2 Characterization

FTIR spectra were recorded using a Nicolet IS10 infrared spectrometer. Solution ^{1}H NMR and solid-state ^{11}B NMR spectra were recorded using a Bruker Avance III 600 spectrometer. DSC and TGA measurements were carried out by using a TA Q200 differential scanning calorimeter. Dynamic mechanical testing was carried out by using a TA Q800 dynamic mechanical analyzer. Mechanical property tests were carried out by using DDL-100, CSS-44050 and MTS landmark machines. SEM images were obtained using a JEOL 6390LV instrument.

2.3 Synthesis of the borate ester-containing curing agent NBO

Under the protection of nitrogen, 3-aminophenylboronic acid (20 g), pentaerythritol (9.9 g) and magnesium sulfate (64 g) were dissolved in 500 mL of tetrahydrofuran. The reaction solution was stirred at room temperature for 24 h. After the reaction was over, the precipitate was removed by filtration, and washed twice using tetrahydrofuran. The organic solution was dried by rotary evaporation to obtain a light-yellow solid. Dichloromethane was added to dissolve the yellow solid under moderate heating, and then petroleum ether was added for recrystallization. After filtration and drying, 22 g of white solid product, **NBO**, was obtained. The yield was 89%.

2.4 Preparation of the E51-NBO vitrimer

The **E51** epoxy resin and the **NBO** curing agent were mixed at a mass ratio of 100 : 42. The mixture then underwent thorough grinding and dispersion using a three-roll mill, and then the **E51-NBO** prepolymer was placed in a vacuum oven and heated to 60 °C under vacuum to eliminate air bubbles. Subsequently, the resin melt was poured into a mold and subjected to a curing process in the oven, following a curing protocol of 120 °C/1 h–150 °C/1 h–180 °C/1 h. Upon natural cooling, the resin-cast body of the **E51-NBO** vitrimer was obtained.

2.5 Preparation of the E51-NBO-IMZ vitrimer

The **NBO** curing agent and imidazole solid were dissolved in acetone with a molecular weight ratio of 10 : 1. After stirring at room temperature for 2 h, the solution was dried by rotary evaporation to obtain a uniform mixture of **NBO-IMZ**. The material ratio and preparation procedures of the **E51-NBO-IMZ** vitrimer were consistent with those of the **E51-NBO** vitrimer.

2.6 Preparation of carbon fiber-reinforced vitrimer composites

The **E51-NBO-IMZ** vitrimer prepolymer was dissolved in acetone at room temperature with a solid content of 50%. Upon complete dissolution, the resin solution was uniformly applied onto the carbon fiber fabric by brushing. Upon complete evaporation of the solvent, the vitrimer prepregs were obtained. The carbon fiber-reinforced vitrimer composites were subsequently fabricated using a compression molding technique.

3. Results and discussion

3.1 Characterization of the E51-NBO and E51-NBO-IMZ vitrimers

In order to improve the heat resistance and mechanical properties of the B–O bond-based epoxy vitrimers, an **NBO** diamine curing agent with a relatively rigid structure and containing a pair of dynamic boronic ester bonds was designed and synthesized. The chemical structure of the **NBO** diamine curing agent was determined by ^{1}H NMR, ^{13}C NMR and ESI mass spectroscopy (Fig. S1–S3). Through common blending and curing processes with the **E51** epoxy resin, two kinds of epoxy vitrimers with and without the N-donor imidazole were fabricated, respectively, designated as **E51-NBO-IMZ** vitrimer and **E51-NBO** vitrimer.

The chemical structures and thermal and mechanical properties of the two vitrimers were characterized and analyzed comparatively. As shown in the FTIR spectra (Fig. 2a), the cured **E51-NBO-IMZ** vitrimer and **E51-NBO** vitrimer exhibited similar chemical cross-linking structures. The amino groups in the **NBO** cross-linker underwent a ring-opening reaction with the epoxy groups in **E51**. Therefore, in the FTIR spectra of the vitrimers, the signals of the amino groups at 3433 cm^{-1} and 3359 cm^{-1} disappeared, as well as the signals of the epoxy groups at 910 cm^{-1}, indicating the occurrence of effective cross-linking reactions. In addition, variable-temperature FTIR spectroscopy was applied to characterize the dynamic exchange properties of the vitrimers (Fig. S4). With an increase of temperature, the signals of B–O bonds at around 1305 cm^{-1} and 1430 cm^{-1} showed no obvious change of peak shape and intensity, indicative of a fast exchange process in the vitrimer. The fast exchange feature also contributed to excellent thermomechanical properties because of the maintenance of the cross-linked network density.

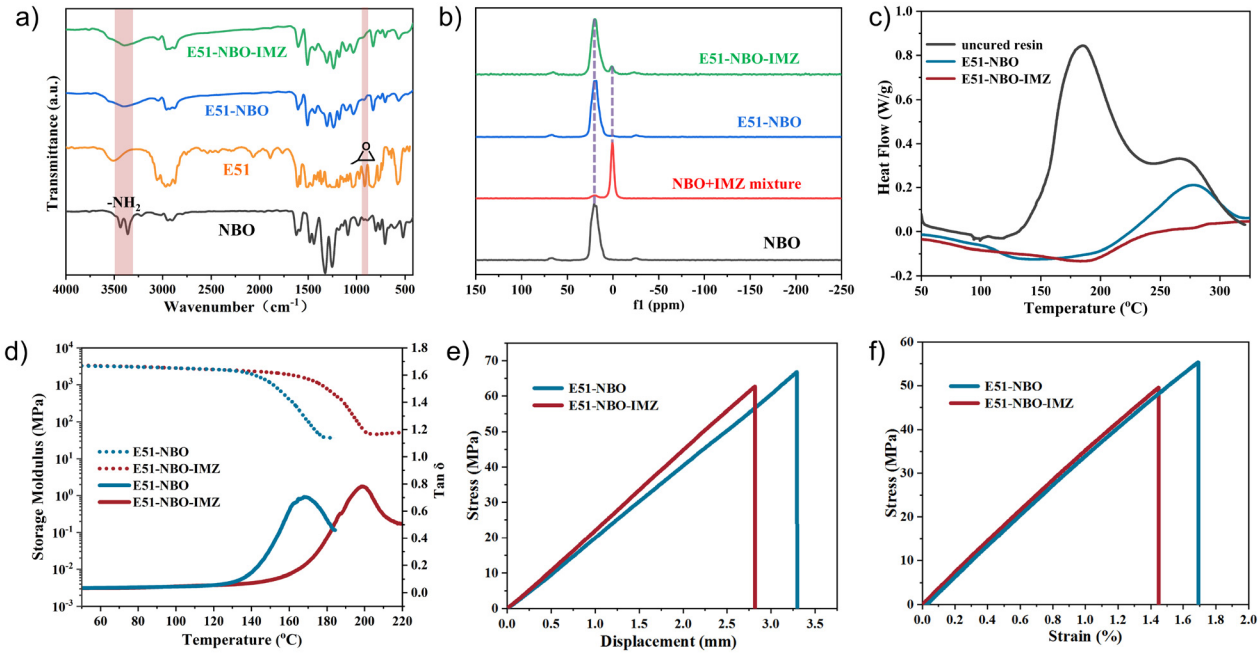

Fig. 2 (a) FTIR spectra of **NBO**, **E51**, the **E51-NBO** vitrimer and the **E51-NBO-IMZ** vitrimer; (b) solid-state ^{11}B NMR spectra of **NBO**, the **NBO** + **IMZ** mixture, the **E51-NBO** vitrimer and the **E51-NBO-IMZ** vitrimer; and (c) the DSC curves of the uncured resin, **E51-NBO** vitrimer and **E51-NBO-IMZ** vitrimer. (d) DMA curves, (e) flexural properties, and (f) tensile properties of the **E51-NBO** vitrimer and **E51-NBO-IMZ** vitrimer.

To verify the presence of the dative N–B interactions in the **E51-NBO-IMZ** vitrimer, solid-state ^{11}B NMR spectroscopy was carried out (Fig. 2b). The ^{11}B NMR spectrum of **NBO** showed a single peak at around 20 ppm, which corresponded to the sp^2 boron atoms in the boronic esters. In the equimolar mixture of **NBO** and **IMZ**, the majority of the ^{11}B signals shifted to around 0.8 ppm, which was consistent with the sp^3 boron atoms involving N–B coordination.[56,57] The spectrum of the **E51-NBO** vitrimer was nearly the same as that of **NBO**, revealing a similar chemical environment of the boron centers in the vitrimer. In the spectrum of the **E51-NBO-IMZ** vitrimer, a weak-signal peak at 1.0 ppm appeared, showing the N–B coordination in the vitrimer upon the addition of **IMZ**.

Differential scanning calorimetry (DSC) analysis was utilized to characterize the residual reaction heat and curing degree. As shown in Fig. 2c, the DSC curve of the uncured resin showed a broad endothermic peak from 140 °C to 300 °C. After the curing reaction process, the endothermic peak of the vitrimers significantly decreased. What differs is that the endothermic peak of the **E51-NBO-IMZ** vitrimer completely disappears, while the **E51-NBO** vitrimer retains a partial endothermic peak at around 250 °C. After post-curing treatment, an endothermic peak in the DSC curve of the **E51-NBO** vitrimer is still present (Fig. S5). Therefore, it was shown that the addition of the **IMZ** accelerator can help enhance the curing reaction activity and increase the cross-linking density, leading to better stability and thermomechanical properties.

Following the research on structural characteristics, the thermal properties of the **E51-NBO** vitrimer and **E51-NBO-IMZ** vitrimer were measured. According to the DMA results (Fig. 2d), the **E51-NBO-IMZ** vitrimer exhibited a glass transition temperature (T_g) of 198 °C, which was 30 °C higher than that of the **E51-NBO** vitrimer (168 °C). The much better thermomechanical properties were attributed to its high-strength cross-linked structure. Despite the significant difference in T_g, the thermogravimetric properties of the two vitrimers were essentially identical due to the same monomeric structures (Fig. S6).

Flexural and tensile tests were carried out to evaluate the mechanical performance of the two epoxy vitrimers (Fig. 2e and f). The flexural modulus and strength of the **E51-NBO** vitrimer were 3.54 GPa and 66.8 MPa, and the tensile modulus and strength were 3.71 GPa and 55.2 MPa. On account of the high rigidity, the **E51-NBO-IMZ** vitrimer showed a higher flexural modulus (3.87 GPa) but a lower flexural strength (62.6 MPa). The tensile modulus of the **E51-NBO-IMZ** vitrimer was almost the same as that of the **E51-NBO** vitrimer, yet the tensile strength was lower (50.0 MPa) due to the decreased elongation at break.

These test results demonstrated that the mechanical performance of such B–O bond-based epoxy vitrimer systems was comparable to that of engineering-grade epoxy resin materials, showing their excellent application potential.[58]

3.2 Thermally active dynamic properties of the E51-NBO and E51-NBO-IMZ vitrimers

The dynamic exchange properties of two vitrimers were investigated through thermally induced stress relaxation experiments. As shown in Fig. 3a and d, the relaxation rate of the vitrimers significantly accelerated with increasing temperature.

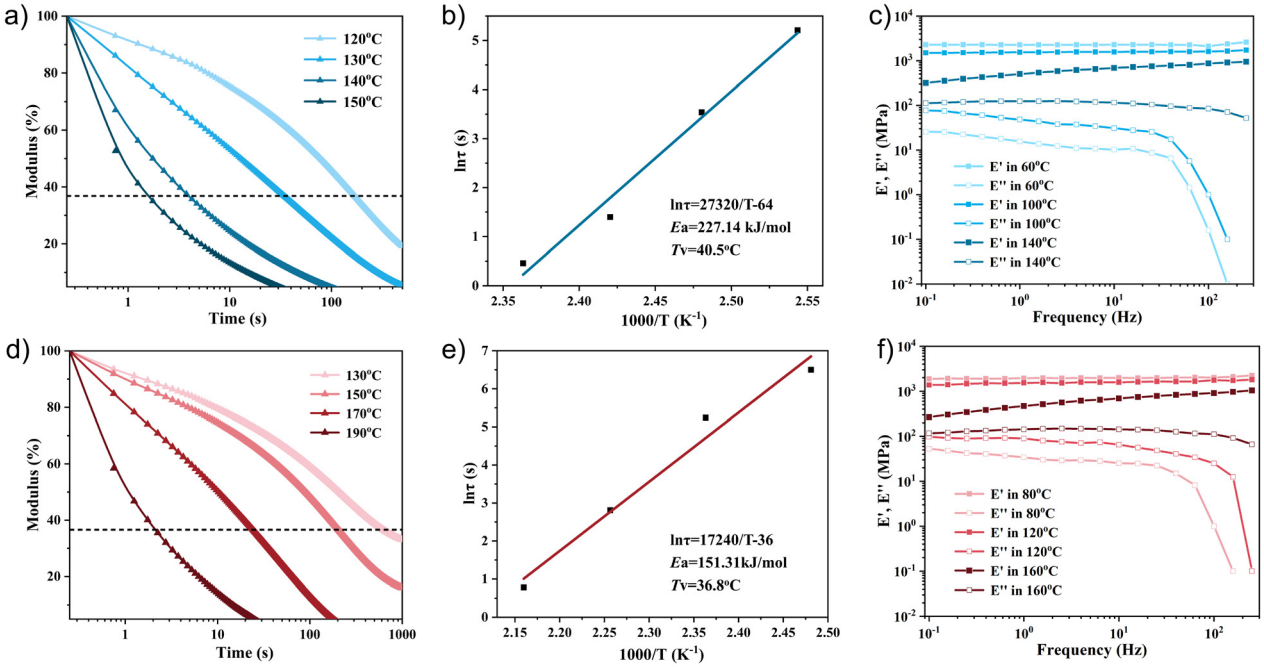

Fig. 3 The stress relaxation curves at various temperatures for (a) the **E51-NBO** and (d) **E51-NBO-IMZ** vitrimers. Linear regression of the logarithm of relaxation time ln(τ) *versus* the reciprocal of temperature (1/T) for (b) the **E51-NBO** and (e) **E51-NBO-IMZ** vitrimers. DMA frequency sweep curves of (c) the **E51-NBO** and (f) **E51-NBO-IMZ** vitrimers at different temperatures.

According to the Maxwell model, the relaxation time was defined as the time when the modulus reduced to 1/e (*i.e.*, 36.8%) of the initial modulus. The relaxation time (τ) of the **E51-NBO** vitrimer at 120 °C was 170 s, which decreased to 1.6 s at 150 °C. Due to its enhanced thermoresistance property, the decrease in relaxation time of the **E51-NBO-IMZ** vitrimer required higher temperatures. With the temperature being increased from 130 °C to 190 °C, the relaxation time of the **E51-NBO-IMZ** vitrimer decreased from 616 s to 2.0 s. Correspondingly, the variations in creep behavior at different temperatures also confirmed the accelerated dynamic exchange properties (Fig. S7).

Based on the results of the stress relaxation experiments, the activation energy (E_a) can be calculated by fitting data according to the Arrhenius equation:[59,60]

$$\tau(T) = \tau_0 \exp(E_a/RT), \quad (1)$$

where τ is the relaxation time, E_a is the activation energy, R is the universal gas constant (8.314 J mol^{-1} K^{-1}), and T is the temperature. The linear fitting function of ln(τ) *vs.* 1000/T is shown in Fig. 3b and e, which indicated that the relaxation times of the **E51-NBO** and **E51-NBO-IMZ** vitrimers were in accordance with the Arrhenius law. The calculated E_a for the **E51-NBO** and **E51-NBO-IMZ** vitrimers were 227.14 kJ mol^{-1} and 151.31 kJ mol^{-1}, respectively, which were higher than those of the published low T_g systems.[61,62] Surprisingly, the **E51-NBO-IMZ** vitrimer exhibited a higher T_g but a lower E_a. It was assumed that, on the one hand, the higher curing degree of the **E51-NBO-IMZ** vitrimer resulted in a higher density of boronic ester dynamic exchange sites in the cross-linked networks. On the other hand, the N–B coordination provided by **IMZ** could help in stabilizing the transition state intermediate, thereby accelerating the equilibrium of the dynamic exchange reaction upon heating. In addition to E_a, the topological freezing transition temperature (T_v) was another important parameter to represent the dynamic exchange activity of the vitrimers. Referring to the calculation method in ref. 63, the T_v values of the **E51-NBO** and **E51-NBO-IMZ** vitrimers were determined to be 40.5 °C and 36.8 °C, respectively. This showed that such B–O bond-based vitrimers possessed the nature to dynamically exchange at near room temperature, but the bond-exchange reaction was also restricted by the segmental mobility related to T_g. Due to the identical dynamic covalent structures, there was not much difference in T_v values between the **E51-NBO** and **E51-NBO-IMZ** vitrimers.

The DMA frequency sweep experiments on the **E51-NBO** vitrimer and **E51-NBO-IMZ** vitrimer were carried out at different temperatures to test their stability with respect to increasing frequencies. Taking into account the difference in T_g of the two vitrimers, the test temperatures of the **E51-NBO** vitrimer were 60 °C, 100 °C and 140 °C, while the test temperatures of the **E51-NBO-IMZ** vitrimer were 80 °C, 120 °C and 160 °C. As shown in Fig. 3c and f, with the increase in temperature, the initial storage modulus (E') of the two vitrimers decreased and the initial loss modulus (E'') exhibited a slight elevation. At lower temperatures, as the scanning frequency increased, the E' of the two vitrimers remained stable, while the E'' sharply dropped to near 0 MPa when the frequency reached above 100 Hz. Compared with the **E51-NBO-IMZ** vitri-

mer, the E'' of the **E51-NBO** vitrimer began to decline at lower frequency (40 Hz). When the temperature approached to around the topological exchange temperature of these vitrimers, their E' values gradually increased as the frequency increased, representing the suppression of molecular chain motions at high oscillation frequency and enhancement of the rigidity. Besides, the E'' values of the two vitrimers exhibited higher stability at high temperatures. The above experimental results indicated that this kind of epoxy vitrimer had relative stability with respect to frequency, but sensitivity to temperature. Furthermore, the addition of imidazole had no significant effect on the frequency responsiveness of the vitrimers.

Furthermore, flexural tests at varying temperatures were applied to characterize the mechanical property variations of the **E51-NBO** and **E51-NBO-IMZ** vitrimers under elevated thermal conditions (Fig. S8). With the temperature increased from 25 °C to 180 °C, the modulus of the vitrimers decreased at an increasingly rapid rate. The modulus of the **E51-NBO** vitrimer experienced a sharp decline at 150 °C, while that of the **E51-NBO-IMZ** vitrimer was at 180 °C. At above 180 °C, the modulus of the vitrimers declined to nearly zero, indicating that the deformation and dynamic exchange reactions could effectively occur at around 180 °C, which was the foundation for self-repairable and deformable performance under heating conditions.

3.3 Solvent resistance of the E51-NBO and E51-NBO-IMZ vitrimers

A series of solvent resistance tests were conducted to characterize and compare the decomposition and swelling performance of the **E51-NBO** vitrimer and **E51-NBO-IMZ** vitrimer in different solvents. Considering the sensitivity of the B–O bonds to protic environments and the vulnerability of epoxy resins to highly polar solvents, we rationally selected four representative solvents: the medium polar protic ethanol, the highly polar protic water, the medium polar aprotic tetrahydrofuran (THF), and the highly polar aprotic *N*,*N*-dimethylformamide (DMF). After being immersed in solvents for 48 h, the **E51-NBO** vitrimer and **E51-NBO-IMZ** vitrimer exhibited highly contrasting solvent resistance performances (Fig. 4). In medium polar protic ethanol, there were no obvious changes in the appearance and volume of the two vitrimers. In highly polar protic water, the outer layer of the **E51-NBO** vitrimer block gradually turned white and became rough, with the volume slightly increased, indicating that the B–O bond-based cross-linked structure underwent a slow process of decomposition in water. In highly polar organic solvents THF and DMF, the **E51-NBO** vitrimer exhibited significant swelling over time, and its volume increased to more than double after 48 hours. In DMF, the outer layer was almost dissolved, due to the synergistic effect of swelling and chemical bond decomposition. In contrast, the **E51-NBO-IMZ** vitrimer exhibited little to no change in these solvents after 48 h, showing the key role of N–B coordination in enhancing the chemical stability of the vitrimer. After about a week, the outer layer of the **E51-NBO-IMZ** vitrimer exhibited slight swelling, whereas the **E51-NBO** vitrimer was almost completely dissolved in DMF (Fig. S9).

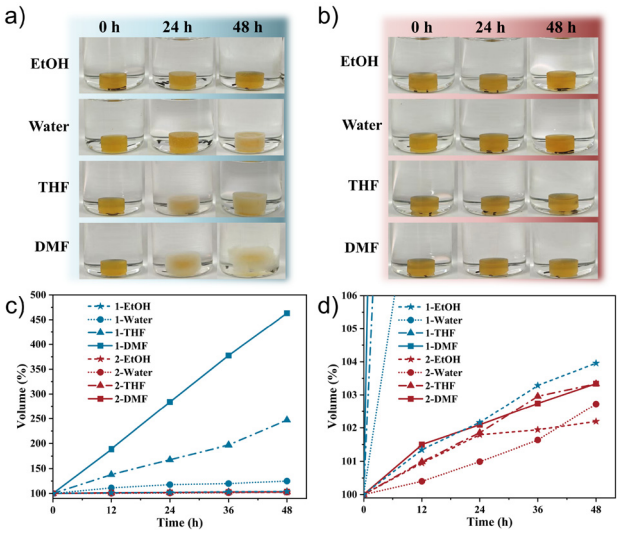

Fig. 4 Photographs of (a) the **E51-NBO** and (b) **E51-NBO-IMZ** vitrimers in different solvents for 0 h, 24 h and 48 h. The volume variation over time of (c) the **E51-NBO** and (d) **E51-NBO-IMZ** vitrimers in different solvents.

To characterize their performance after the solvent resistance tests, DMA and flexural test samples of the **E51-NBO** and **E51-NBO-IMZ** vitrimers were prepared and placed in different solvents (EtOH, water, THF and DMF) for 24 hours. After that, the thermal and mechanical properties of the samples were measured. Due to the significant swelling of and degradation effect on the **E51-NBO** vitrimer in DMF, its samples in DMF did not qualify for testing. As shown in Fig. S10a and S10c, the heat resistance and mechanical properties of the **E51-NBO** vitrimer both decreased significantly after solvent immersion. Its initial storage modulus exhibited significant decrease and its T_g decreased from 168 °C to 164 °C (in EtOH), 152 °C (in water) and 137 °C (in THF), respectively. Meanwhile, its flexural strength and flexural modulus also decreased significantly, especially for the sample immersed in THF. The decline in the thermal and mechanical performance of the **E51-NBO** vitrimer was consistent with the results of its solvent resistance test. As for the **E51-NBO-IMZ** vitrimer (Fig. S10b and S10d), the T_g, flexural strength and flexural modulus were all well maintained, which indicated the excellent solvent resistance performance of the B–O bond-based epoxy vitrimer after the addition of imidazole.

3.4 Recycling performance of the E51-NBO-IMZ vitrimer

Comprehensive performance characterization has proven that the **E51-NBO-IMZ** vitrimer system containing the N-donor imidazole possessed superior thermomechanical properties and enhanced stability, thereby presenting greater potential for engineering applications. To validate the feasibility of the **E51-NBO-IMZ** vitrimer in recyclable, repairable and degradable epoxy resin-based materials, a series of experiments were carried out.

To verify the recyclability and processability of the **E51-NBO-IMZ** vitrimer, the cured vitrimer was smashed into fine particles and underwent a reforming process through hot mould pressing at 180 °C and 5 MPa for 1 h. The second and third recycled samples were prepared *via* the same process. To evaluate the retention of mechanical properties of the vitrimer after recycling, the tensile properties of pristine and recycled vitrimer samples were tested. The stress–strain curves are shown in Fig. 5b, and the histograms of tensile strength and tensile modulus are shown in Fig. 5c. The **E51-NBO-IMZ** vitrimer exhibited monotonously decreased tensile strength as the reprocessing cycles increased. The retention rate of tensile strength was 89% after the first recycling, which reduced to 76% after the third recycling. Nevertheless, there was no significant reduction in the tensile modulus of the original and reprocessed vitrimers. The reason the tensile strength decreased as the number of recycling times increased was that, on the one hand, during the re-molding process after smashing, microdefects or pores gradually accumulated inside the resin, making it prone to failure under load. On the other hand, the epoxy resin underwent a certain degree of aging after repeated hot-pressing. The effect of aging on the tensile strength was relatively significant, while its impact on the tensile modulus was not obvious. The high retention rate of the tensile modulus after multiple reprocessing cycles was mainly due to the fact that the cross-linking density and rigidity of the vitrimer did not change significantly after multiple curing processes, which indicated the efficient dynamic exchange and reconstruction of the borate ester bond networks that occurred during the recycling process.

3.5 Self-repairing performance of the E51-NBO-IMZ vitrimer

Taking advantage of the dynamic exchange activity of the **E51-NBO-IMZ** vitrimer at high temperature, a series of self-repairing tests on cured vitrimer and CFRCs were conducted. To show that the self-repair can be achieved under low pressure, a self-repair device based on a vacuum bag was designed (as illustrated in Fig. 6a). Artificial damage, taking surface scratches and impact cracks as examples, were created on the cured vitrimer samples. Then, the samples were placed under 200 °C and 0.1 MPa vacuum conditions for 10 min. Then, scanning electron microscopy (SEM) and microfocus computed tomography (CT) were employed to characterize the surface morphology and internal quality of the damaged and repaired vitrimer samples. As shown in Fig. 6b and c, after a short period of softening and chemical bond exchanging at high temperature and under vacuum pressure, both the surface and internal defects of the **E51-NBO-IMZ** vitrimer were well repaired. Due to the uneven shaping effect of the peel ply and vacuum bag, corresponding wrinkles and deformations appeared on the samples, proving that the plastic deformations effectively occurred on the vitrimer. In contrast, self-repairing experiments of shorter duration were carried out and showed only partially repaired damage (Fig. S11), indicating that the defects need sufficient processing time to be fully repaired.

Besides, the self-repair performance of carbon fiber-reinforced vitrimer composites was also tested (Fig. 6d and e). Two kinds of composite specimens respectively with delamination and loose defects were intentionally fabricated, which represented two common types of imperfections encountered during composite manufacturing processes. Following the same self-repairing procedures, the two defective composite specimens exhibited effective self-repairing capabilities,

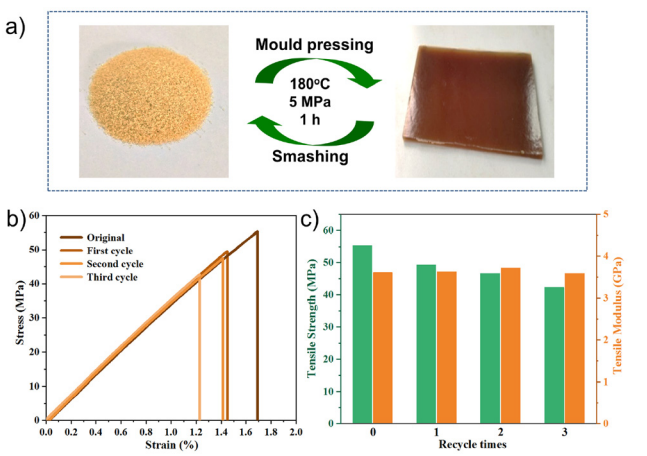

Fig. 5 (a) Illustration of the recycling and reprocessing of the **E51-NBO-IMZ** vitrimer. (b) Tensile curves of the original and recycled vitrimers. (c) Tensile strength and tensile modulus of the original and recycled vitrimers.

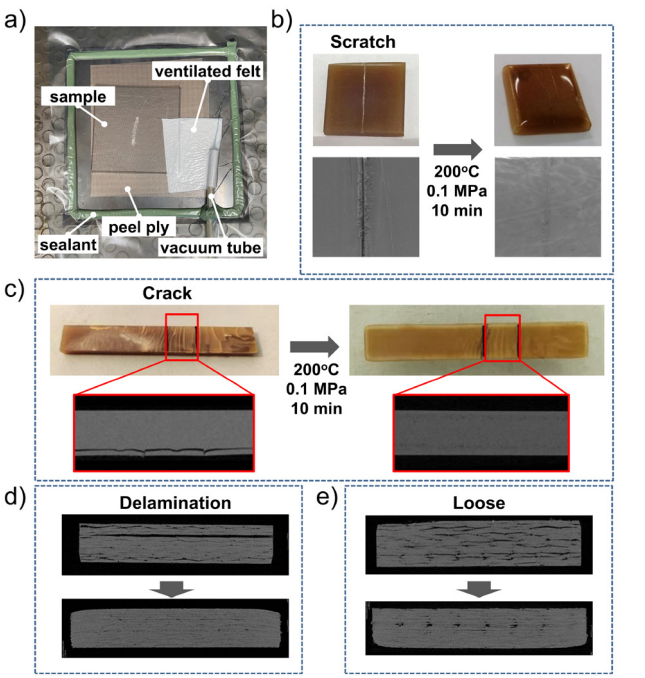

Fig. 6 (a) Vacuum setup for the self-repairing experiment. (b–e) Characterization before and after the self-repair of the damaged **E51-NBO-IMZ** vitrimer and composites.

accompanied by a slight reduction in thickness. In addition, the flexural properties of the CFRC samples before and after self-repairing were measured (Fig. S12). The flexural strength and modulus of the loose specimen were both significantly improved after self-repairing. For the delamination defective specimen, the flexural strength was enhanced more significantly. Thus, it is demonstrated that the CFRCs can achieve efficient self-repair of internal qualities and mechanical properties after rapid heating and vacuum treatments.

The above experiments showed that the **E51-NBO-IMZ** vitrimer and its composites possessed efficient self-repairing properties at high temperatures and under appropriate pressure, showing application potential in the field of reusable fiber-reinforced composite components.

3.6 Degradability and carbon fiber recyclability of E51-NBO-IMZ vitrimer-based composites

According to the results of the solvent resistance tests, the **E51-NBO-IMZ** vitrimer exhibited excellent anti-swelling properties and chemical stability toward highly polar and protic environments. This was attributed to the high cross-linking density and dative N–B interactions resulting from the addition of **IMZ**. To verify whether it can degrade in solvents and can be used as the matrix for degradable composite materials, we combined the polar solvent (DMF) with an acidic protonic solvent (HCl aqueous solution) for the degradation experiment on the **E51-NBO-IMZ** vitrimer, leveraging the synergistic effect of swelling and B–O bond cleavage.[64,65] The reaction mechanism was such that the boronic ester groups in the vitrimer could be hydrolyzed into boric acid in an acidic aqueous solution, leading to the dissociation of the cross-linked networks (Fig. S13). As shown in Fig. 7a, the vitrimer block experienced a gradual dissolution process over time and the solvent became turbid, revealing that such a mixed solvent system was practicable for the degradation of the **E51-NBO-IMZ** vitrimer. In order to test whether the **E51-NBO-IMZ** vitrimer in CFRCs could be effectively degraded, a strip-shaped composite specimen was prepared, of which the lower half was immersed in the same mixed solvent (Fig. 7b). After approximately one day, with the assistance of stirring, the immersed

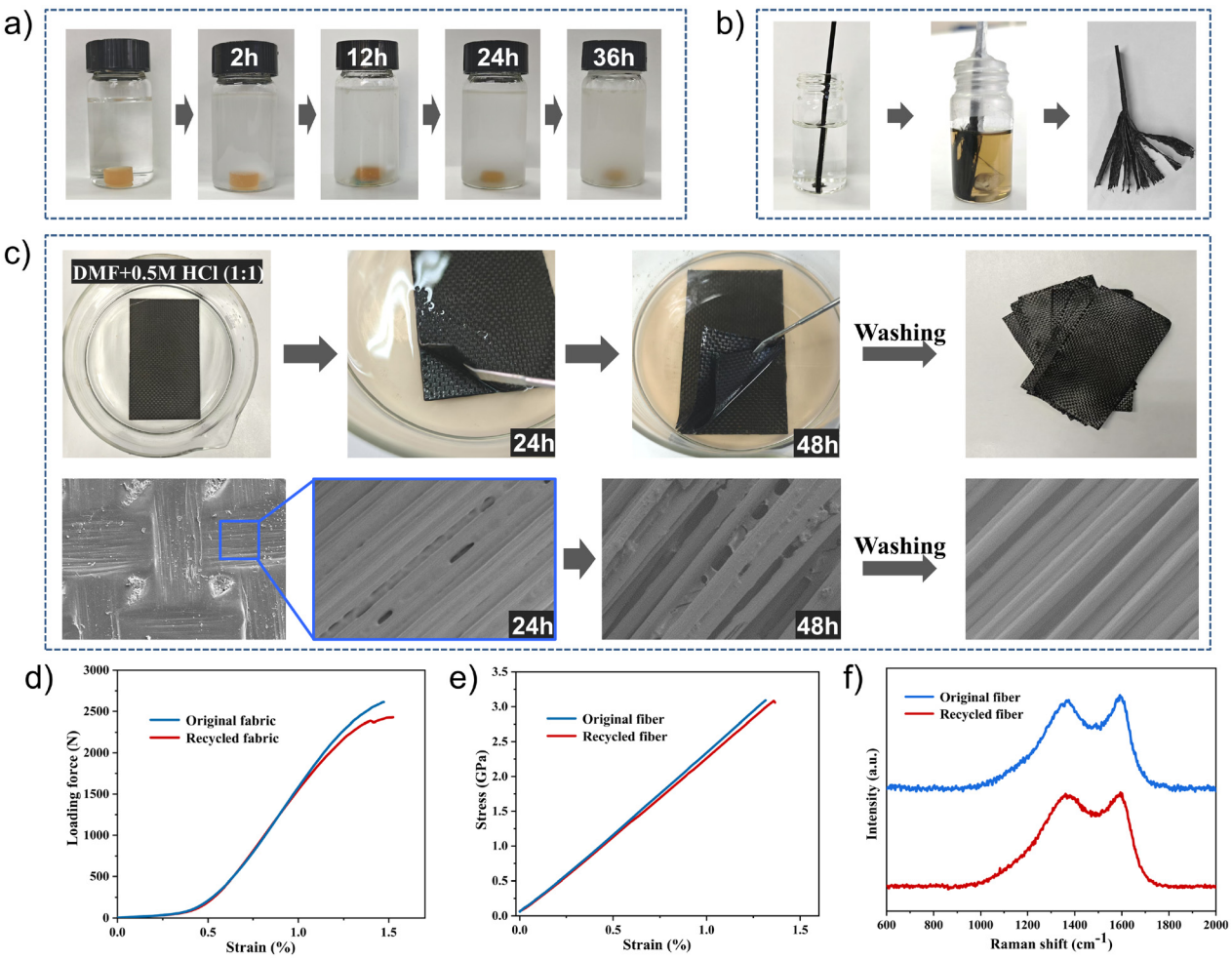

Fig. 7 (a) Degradation of the **E51-NBO-IMZ** vitrimer block in the DMF/HCl mixed solvent. (b) Degradation of the **E51-NBO-IMZ** vitrimer in CFRCs. (c) Recycling of the carbon fiber fabric in the DMF/HCl mixed solvent. (d) Fabric tensile curves, (e) fiber tensile curves, and (f) Raman spectra of the original and recycled carbon fibers.

part of the composite exhibited significant softening and delamination. After cleaning and drying, the carbon fiber fabric could be easily and completely separated, which verified the feasibility of carbon fiber recycling.

On this basis, a CFRC plate was prepared and immersed in the mixed solvent. The microscopic changes on the carbon fibers were characterized by SEM (Fig. 7c). After 24 hours, the edges of the composite plate softened and became partially delaminated, and the carbon fibers were exposed as the vitrimer on the surface was degraded and dissolved. After 48 hours, the carbon fiber fabric in the composite plate could be easily peeled off layer by layer, and the vitrimer between or inside the carbon fibers was also significantly degraded. Following the cleaning and drying treatments, the carbon fiber fabrics were completely recycled. Moreover, tensile tests and Raman spectroscopy were employed to evaluate the mechanical properties and structural quality of the recycled carbon fibers. As shown in Fig. 7d and e, the modulus and strength of the recycled carbon fiber and fabric were close to those of the original carbon fiber and fabric, but there was a slight decline under high loads. In conducting Raman spectroscopy (Fig. 7f), it was shown through spectra that the recycled carbon fiber exhibited consistent curves and peak intensities compared with those of the original carbon fiber. The I_D/I_G intensity ratio increased from 0.96 to 0.97, representing a very slight increase in carbon fiber defects.[66,67] These phenomena indicated that the **E51-NBO-IMZ** vitrimer-based CFRCs could be recycled and maintain their mechanical properties and structural quality.

4. Conclusions

In summary, a novel borate ester bond-based epoxy vitrimer with improved stability and thermomechanical and thermally activated dynamic exchange properties was constructed and studied. A high epoxy value monomer and high rigidity diamine curing agent containing B–O bonds were employed for the fabrication of a high-performance epoxy vitrimer. Besides, a small amount of imidazole was added to introduce the N–B coordination interactions that could stabilize the sensitive B–O bonds. Owing to the promoting effect of imidazole on the epoxy ring opening reaction, the **E51-NBO-IMZ** vitrimer exhibited enhanced cross-linking strength, leading to higher modulus and T_g (198 °C) values. Furthermore, the stress relaxation tests revealed that the **E51-NBO-IMZ** vitrimer had a lower E_a (151.31 kJ mol^{-1}), suggesting a better dynamic exchange performance at elevated temperatures. In addition, the dative N–B interactions yielded the **E51-NBO-IMZ** vitrimer with remarkable solvent resistance compared to the **E51-NBO** vitrimer. The effectively dynamic B–O bond networks endowed the **E51-NBO-IMZ** vitrimer with excellent recyclability, degradability and self-repairing properties under appropriate heating, stress and chemical conditions. All the aforementioned research of the N–B coordination-enhanced B–O bond-based vitrimer makes it attractive for the fabrication of engineering-applicable high-performance vitrimer-based composites. By altering the structure of epoxy monomers and curing agents, a large variety of self-repairing and recyclable epoxy-based composites with pre-designed functions and properties can be generated.

Conflicts of interest

There are no conflicts to declare.

Data availability

All data supporting the findings of this study are within the paper and its SI.

Supplementary information presents the structural characterization of NBO curing agent, the DSC, TG, creep curves, and flexural curves of vitrimers, the properties of vitrimers before and after solvent resistance testing and self-repair testing. See DOI: https://doi.org/10.1039/d5lp00144g.

Acknowledgements

The authors gratefully acknowledge the support towards this research from the National Natural Science Foundation (no. 51903229 and 52303164).

References

1 V. Schenk, K. Labastie, M. Destarac, P. Olivier and M. Guerre, *Mater. Adv.*, 2022, **3**, 8012–8029.
2 S. Utekar, V. K. Suriya, N. More and A. Rao, *Composites, Part B*, 2021, **207**, 108596.
3 A. Dorigato, *Adv. Ind. Eng. Polym. Res.*, 2021, **4**, 116–132.
4 D. Montarnal, M. Capelot, F. Tournilhac and L. Leibler, *Science*, 2011, **334**, 965–968.
5 J. Zhang, V. S. Chevali, H. Wang and C. H. Wang, *Composites, Part B*, 2020, **193**, 108053.
6 Y. Yuan, Y. Sun, S. Yan, J. Zhao, S. Liu, M. Zhang, X. Zheng and L. Jia, *Nat. Commun.*, 2017, **8**, 14657.
7 B. Qin, S. Liu and J.-F. Xu, *Angew. Chem., Int. Ed.*, 2023, **62**, e202311856.
8 W. Denissen, J. M. Winne and F. E. Du Prez, *Chem. Sci.*, 2016, **7**, 30–38.
9 J. M. Winne, L. Leibler and F. E. Du Prez, *Polym. Chem.*, 2019, **10**, 6091–6108.
10 P. Chakma and D. Konkolewicz, *Angew. Chem., Int. Ed.*, 2019, **58**, 9682–9695.
11 Z. P. Zhang, M. Z. Rong and M. Q. Zhang, *Prog. Polym. Sci.*, 2018, **80**, 39–93.
12 T. Yang, X. Lu, X. Wang, X. Wei, N. An, Y. Li, W. Wang, X. Li, X. Fang and J. Sun, *Angew. Chem., Int. Ed.*, 2024, **63**, e202403972.
13 X. Lu, L. Guo, Y. Wang and J. Sun, *Adv. Funct. Mater.*, 2025, **35**, 2503106.

14 Y. Wu, Y. Wei and Y. Ji, *Giant*, 2023, **13**, 100136.
15 S. Weidmann, P. Volk, P. Mitschang and N. Markaide, *Composites, Part A*, 2022, **154**, 106791.
16 P. R. Barnett, J. A. Brackenridge, A. A. Advincula, L. A. Taussig and D. Nepal, *Composites, Part B*, 2024, **274**, 111270.
17 Y. Zhang, H. Yan, R. Yu, J. Yuan, K. Yang, R. Liu, Y. He, W. Feng and W. Tian, *Adv. Sci.*, 2023, 2306350.
18 Y. Yang, Y. Xu, Y. Ji and Y. Wei, *Prog. Mater. Sci.*, 2021, **120**, 100710.
19 W. Li, L. Xiao, J. Huang, Y. Wang, X. Nie and J. Chen, *Compos. Sci. Technol.*, 2022, 109575.
20 Y. Xu, H. Zhang, S. Dai, S. Xu, J. Wang, L. Bi, J. Jiang and Y. Chen, *Compos. Sci. Technol.*, 2022, **228**, 109676.
21 H. Zhang and X. Xu, *Composites, Part A*, 2017, **99**, 15–22.
22 K. Yu, Q. Shi, M. L. Dunn, T. Wang and H. J. Qi, *Adv. Funct. Mater.*, 2016, **26**, 6098–6106.
23 B. Li, G. Zhu, Y. Hao, R. Li, X. Zhang and X. Guo, *J. Polym. Sci. (Hoboken, NJ, U. S.)*, 2024, **62**, 1468–1479.
24 Q. Zhou, X. Zhu, W. Zhang, N. Song and L. Ni, *ACS Appl. Polym. Mater.*, 2020, **2**, 1865–1873.
25 J. Xu, W. Sun, Y. Liang, Y. Cheng and L. Zhang, *Polymer*, 2023, **283**, 126233.
26 J. Tellers, R. Pinalli, M. Soliman, J. Vachon and E. Dalcanale, *Polym. Chem.*, 2019, **10**, 5534–5542.
27 W. Denissen, G. Rivero, R. Nicolaÿ, L. Leibler, J. M. Winne and F. E. Du Prez, *Adv. Funct. Mater.*, 2015, **25**, 2451–2457.
28 T. Debsharma, V. Amfilochiou, A. A. Wróblewska, I. De Baere, W. Van Paepegem and F. E. Du Prez, *J. Am. Chem. Soc.*, 2022, **144**, 12280–12289.
29 M. O. Saed and E. M. Terentjev, *ACS Macro Lett.*, 2020, **9**, 749–755.
30 X. Wu, X. Yang, R. Yu, X.-J. Zhao, Y. Zhang and W. Huang, *J. Mater. Chem. A*, 2018, **6**, 10184–10188.
31 B. Strachota, J. Hodan, J. Dybal and L. Matejka, *Macromol. Mater. Eng.*, 2020, **306**, 2000474.
32 K. Sugane, R. Takagi and M. Shibata, *React. Funct. Polym.*, 2018, **131**, 211–218.
33 E. Trovatti, T. M. Lacerda, A. J. Carvalho and A. Gandini, *Adv. Mater.*, 2015, **27**, 2242–2245.
34 X. Kuang, Y. Zhou, Q. Shi, T. Wang and H. J. Qi, *ACS Sustainable Chem. Eng.*, 2018, **6**, 9189–9197.
35 M. Capelot, D. Montarnal, F. Tournilhac and L. Leibler, *J. Am. Chem. Soc.*, 2012, **134**, 7664–7667.
36 X. Zhang, S. Wang, Z. Jiang and X. Jing, *J. Am. Chem. Soc.*, 2020, **142**, 21852–21860.
37 H. Memon, Y. Wei, L. Zhang, Q. Jiang and W. Liu, *Compos. Sci. Technol.*, 2020, **199**, 108314.
38 L. Xie, Y. Wang, G. Chen, H. Feng, N. Zheng, H. Ren, Q. Zhao and T. Xie, *Compos. Commun.*, 2021, **28**, 100979.
39 O. R. Cromwell, J. Chung and Z. Guan, *J. Am. Chem. Soc.*, 2015, **137**, 6492–6495.
40 Z.-H. Zhao, C.-H. Li and J.-L. Zuo, *Smart Mater.*, 2023, **4**, e1187.
41 S. Cho, S. Y. Hwang, D. X. Oh and J. Park, *J. Mater. Chem. A*, 2021, **9**, 14630–14655.
42 A. P. Bapat, B. S. Sumerlin and A. Sutti, *Mater. Horiz.*, 2020, **7**, 694–714.
43 C. Kim, H. Ejima and N. Yoshie, *RSC Adv.*, 2017, **7**, 19288–19295.
44 C. Bao, Y.-J. Jiang, H. Zhang, X. Lu and J. Sun, *Adv. Funct. Mater.*, 2018, **28**, 1800560.
45 J. J. Cash, T. Kubo, A. P. Bapat and B. S. Sumerlin, *Macromolecules*, 2015, **48**, 2098–2106.
46 S. Ito, H. Takata, K. Ono and N. Iwasawa, *Angew. Chem.*, 2013, **125**, 11251–11254.
47 W. Zhang, Q. Zhou, C. Fang, X. Yuan, X. Li, Q. He, X. Dong, Y. Qi, B. Wang and W. Li, *J. Polym. Res.*, 2022, **29**, 244.
48 Y. Zeng, J. Li, S. Liu and B. Yang, *Polymers*, 2021, **13**, 2286.
49 J. Teng, X. Shen, G. Hang, Y. Gao, J. Hu and S. Zheng, *ACS Appl. Polym. Mater.*, 2025, **7**, 2716–2730.
50 S. Ren, Z. Li, W. Zhou, J. Zhu, Y. Zhao, C. Liu, H. Fang and Y. Ding, *Ind. Crops Prod.*, 2023, **206**, 117738.
51 W. A. Ogden and Z. Guan, *J. Am. Chem. Soc.*, 2018, **140**, 6217–6220.
52 Y. Li, Y. Chen, B. Hu, P. Tian, C. Zhang, X. Xing and X. Jing, *Polymer*, 2025, **329**, 128509.
53 H. Fang, Y. Zhao, X. Xie, F. Zhang, J. Zhu, S. Ren and Y. Ding, *Polymer*, 2024, **311**, 127587.
54 J. Zheng, Z. Y. Oh, E. Ye, W. H. Chooi, Q. Zhu, X. J. Loh and Z. Li, *Mater. Chem. Front.*, 2023, **7**, 381–404.
55 K. Song, W. Ye, X. Gao, H. Fang, Y. Zhang, Q. Zhang, X. Li, S. Yang, H. Wei and Y. Ding, *Mater. Horiz.*, 2021, **8**, 216–223.
56 K. Song, W. Ye, X. Gao, H. Fang, Y. Zhang, Q. Zhang, X. Li, S. Yang, H. Wei and Y. Ding, *Mater. Horiz.*, 2021, **8**, 216–223.
57 C. Kim, H. Ejima and N. Yoshie, *J. Mater. Chem. A*, 2018, **6**, 19643–19652.
58 D. Sangaletti, L. Ceseracciu, L. Marini, A. Athanassiou and A. Zych, *Resour., Conserv., Recycl.*, 2023, **198**, 107205.
59 Y. Fu, S. Chen, X. Chen, H. Zheng, X. Yan, Z. Liu, M. Wang and L. Liu, *Adv. Funct. Mater.*, 2024, **34**, 2314561.
60 Z. H. Zhao, D. P. Wang, J. L. Zuo and C. H. Li, *ACS Mater. Lett.*, 2021, **3**, 1328–1338.
61 L. Li, J. Xu, Y. Gao, J. Hu and S. Zheng, *React. Funct. Polym.*, 2023, **191**, 105689.
62 Y. Xu, S. Dai, L. Bi, J. Jiang, H. Zhang and Y. Chen, *Chem. Eng. J.*, 2022, **429**, 132518.
63 H. Memon, Y. Wei, L. Zhang, Q. Jiang and W. Liu, *Chem. Sci. Technol.*, 2020, **199**, 108314.
64 B. Wang, S. Ma, X. Xu, Q. Li, T. Yu, S. Wang, S. Yan, Y. Liu and J. Zhu, *ACS Sustainable Chem. Eng.*, 2020, **8**, 11162–11170.
65 S. Kumar and S. Krishnan, *Chem. Pap.*, 2020, **74**, 3785–3807.
66 Z. Jian, Y. Wang, X. Zhang, X. Yang, Z. Wang, X. Lu and H. Xia, *J. Mater. Chem. A*, 2023, **11**, 21231–21243.
67 Y.-Y. Liu, G.-L. Liu, Y.-D. Li, Y. Weng and J.-B. Zeng, *ACS Sustainable Chem. Eng.*, 2021, **9**, 4638–4647.